Chemical Engineering Journal 163 (2010) 395–402

Contents lists available at ScienceDirect

Chemical Engineering Journal

journal homepage: www.elsevier.com/locate/cej

Effect of Mg and Ca addition on coke deposition over Cu–Ni/SiO_2 catalysts for ethanol steam reforming

A. Carrero, J.A. Calles, A.J. Vizcaíno*

Department of Chemical and Energy Technology, ESCET, Universidad Rey Juan Carlos, C/Tulipán s/n, 28933 Móstoles, Madrid, Spain

ARTICLE INFO

Article history:
Received 26 March 2010
Received in revised form 2 July 2010
Accepted 9 July 2010

Keywords:
Ethanol steam reforming
Cu–Ni catalysts
Calcium
Magnesium
Coke characterization

ABSTRACT

The production of hydrogen from ethanol steam reforming with Cu–Ni catalysts supported on MgO- and CaO-modified silica has been studied. Two promoting effects have been found: reduction of the metallic Cu–Ni particles size and strengthening of the metal–support interaction. Moreover, Mg- and Ca-promoted catalysts favour the formation of defective carbon, which is more reactive and thermodynamically easier to be removed during the ethanol steam reforming process. Consequently, higher hydrogen production and lower coke formation are achieved when Cu–Ni catalysts are supported on Mg- or Ca-modified silica in comparison to unmodified Cu–Ni/SiO_2 catalyst. The highest hydrogen selectivity (84.8 mol%) is reached with a Cu–Ni/Mg–SiO_2 catalyst containing 10 wt% Mg, while the incorporation of 10 wt% Ca into Cu–Ni/SiO_2 catalyst reduces considerably the amount of coke deposited from 58.4 to 26.3 wt%, after 3 h of time on stream.

1. Introduction

The environmental problems associated with the intensive use of fossil fuels are increasingly demanding the development of sustainable energy systems. In this sense, hydrogen can be considered as future clean energy vector while produced from renewable resources. Among the potential available alternatives, ethanol steam reforming is a good candidate since it can be produced from biomass (like agricultural wastes) [1]. Moreover, it can be distributed in a logistic net similar to the conventional petrol stations since ethanol is a non-toxic liquid with safe handling, transportation and storage.

Hydrogen production through ethanol steam reforming is an efficient process [2], which can be represented as follows:

$$CH_3CH_2OH + 3H_2O \rightarrow 2CO_2 + 6H_2 \qquad (\Delta H^\circ = +347.4\,kJ/mol)$$

The overall reaction involves several steps such as ethanol dehydrogenation and/or dehydration, which produce acetaldehyde or ethylene as intermediate products, respectively. Decarbonylation or steam reforming of these intermediates generates hydrogen, together with methane and carbon monoxide. Next, methane can go through steam reforming reaction producing carbon monoxide and hydrogen, while the carbon monoxide generated in the aforementioned steps can be transformed into carbon dioxide through the water-gas shift reaction, generating more hydrogen. Moreover, coke can be formed from some intermediate products [3,4].

Cu–Ni supported catalysts have been described in the literature because of their high activity on ethanol steam reforming [2,5–8]. Besides the Cu–Ni active phase, catalytic support plays also an important role since it should favour: (i) metal stability, (ii) ethanol dehydrogenation to acetaldehyde instead of alcohol dehydration to ethylene, and (iii) water activation by the mobility of OH groups to help the reaction with the CH_xO_y fragments adsorbed on the metal particles [7–11].

However, the main drawback of Cu–Ni catalyst is that it can be deactivated easily because of coke deposition, and/or metal particle sintering during the reaction. In this sense, Ni reforming catalysts like Ni/Al_2O_3, have been modified through the incorporation of basic alkaline and earth alkaline oxides elements since the acidity of the support is detrimental to coke formation [12–17]. In a similar way, the amount of deposited coke on Cu–Ni/SBA-15 was significantly reduced throughout the modification of SBA-15 mesostructured silica support with Ca and Mg oxides [18]. Although it is reasonable to think that CaO and MgO incorporation will not only reduce coke amount, but also modify the nature of coke deposited on Ni steam reforming catalysts [15], this has not been deeply reported in the literature yet. For this reason, the aim of this work is the modification of Cu–Ni/SiO_2 catalyst by CaO and MgO to improve their performance on ethanol steam reforming, relating not only the amount but also the type of coke formed with the catalyst properties.

* Corresponding author. Tel.: +34 914888096; fax: +34 914887068.
E-mail address: arturo.vizcaino@urjc.es (A.J. Vizcaíno).

1385-8947/$ – see front matter © 2010 Elsevier B.V. All rights reserved.
doi:10.1016/j.cej.2010.07.029

2. Experimental

2.1. Catalysts preparation

Catalysts containing 2 wt% Cu, 7 wt% Ni and different Ca and Mg loadings, ranging from 0 to 20 wt%, were prepared by incipient wetness impregnation of commercial amorphous silica (Ineos) using aqueous solutions of nitrates ($Cu(NO_3)_2{\cdot}3H_2O$ and $Ni(NO_3)_2{\cdot}6H_2O$ from Scharlab, $Mg(NO_3)_2{\cdot}6H_2O$ and $Ca(NO_3)_2{\cdot}6H_2O$ from Aldrich) as metal precursors. The corresponding alkaline-earth element was impregnated on silica prior to the Cu–Ni phase. The modified supports were then calcined at 550 °C, temperature selected from TG and XRD analyses (performed as described in Section 2.2) for being high enough to lead to total decomposition of the Mg and Ca precursors. After this, simultaneous addition of copper and nickel precursors was carried out, as described elsewhere [7,8], followed by drying overnight and subsequent calcination at 400 °C for 15 h with a heating rate of 1.8 °C min^{-1}. Finally, the catalysts were reduced in the fixed-bed reactor used for catalytic tests under flowing pure hydrogen (30 N mL min^{-1}) at 600 °C for 4.5 h with a heating rate of 2 °C min^{-1}.

Samples were denoted as CuNi/Mx-S, where "CuNi" indicates the presence of the Cu–Ni phase in the catalyst, "M" represents the alkaline-earth element in the sample, "x" is the nominal content of the element in the support and "S" refers to the amorphous silica support. Besides, a $CuNi/SiO_2$ catalyst (2 wt% Cu and 7 wt% Ni) was also prepared as a reference catalyst.

2.2. Characterization of supports and fresh catalysts

Characterization of these materials was performed by TGA, ICP-AES, N_2 adsorption–desorption, XRD, TPR and TEM. Physicochemical changes taking place in the samples as a consequence of temperature were recorded by TGA in airflow (100 mL min^{-1}) on a Mettler Toledo TGA/DSC1 thermobalance, with a heating rate of 5 °C min^{-1} up to 800 °C. Chemical composition was determined by ICP-AES technique using a Varian VISTA-PRO AX spectrophotometer. Previously, solid samples were dissolved by acidic digestion. Textural properties were measured by N_2 adsorption–desorption using a Micromeritics TRISTAR 3000 sorptometer. Prior to the adsorption, samples were outgassed under vacuum at 250 °C for 10 h. Surface areas were calculated according to BET method. Species identification (according to JCPDS index) and mean metallic crystallites size determination (from the Scherrer equation) were performed by powder XRD analyses on a Philips X'PERT PRO diffractometer, using Cu K_α radiation. The diffractometer is equipped with a high-temperature chamber in order to analyse samples in situ at different temperatures. Diffractograms were recorded at $2\theta = 0.020^\circ$ increment step and 2 s collection time. Reduction properties of the calcined samples were determined by TPR measurements, performed on a Micromeritics AUTOCHEM 2910 equipment under 10% H_2 in Ar flow (35 mL min^{-1}) with a heating rate of 5 °C min^{-1} from 25 to 800 °C. Samples were previously degasified under dry Ar flow (35 mL min^{-1}) at calcination temperature. Size and morphology of the supported active phase could be observed by TEM. Micrographs were acquired on a Phillips TECNAI 20 microscope equipped with LaB_6 filament, an accelerating voltage of 200 kV and the possibility to perform elemental microanalysis by energy dispersive X-ray spectroscopy (EDXS). Samples were prepared by powder dispersion of the material, finely divided, in acetone and subsequent deposition on a gold grid with carbon support.

2.3. Catalytic tests

Catalytic tests on ethanol steam reforming were carried out into a fixed-bed reactor connected to an on-line gas chromatograph, as described elsewhere [7,8]. Previously, the calcined catalyst diluted in silicon carbide (catalyst/SiC weight ratio 1:5), was in situ reduced under hydrogen flow at 600 °C for 4.5 h with a heating rate of 2 °C min^{-1}. After activation, catalytic tests were performed for 180 min at atmospheric pressure and 600 °C, feeding a liquid water/ethanol mixture (molar ratio: 3.7) at space velocity WHSV = 12.7 h^{-1}, which was vaporized and then diluted with nitrogen flow (30 mL min^{-1}).

Reactants conversion and products selectivity were calculated as follows:

$$X_{\text{reactant}}\ (\%) = \frac{F_{\text{reactant,in}} - F_{\text{reactant,out}}}{F_{\text{reactant,in}}} \times 100$$

$$S_{H_2}(\%) = \frac{F_{H_2\text{produced}}}{3 \times (F_{\text{ethanol,in}} - F_{\text{ethanol,out}}) + (F_{\text{water,in}} - F_{\text{water,out}})} \times 100$$

$$S_{i\ \text{carbon-containing product}}(\%) = \frac{F_{i\text{carbon-containing product}}}{n_i \times (F_{\text{ethanol,in}} - F_{\text{ethanol,out}})} \times 100$$

$F_{i,\text{in}}$ and $F_{i,\text{out}}$ are the molar flow rate of the i species at the inlet and at the outlet of the reactor, respectively, and n_i is the stoichiometric factor between the carbon-containing products and ethanol.

2.4. Characterization of used catalysts

Carbon deposited during reaction on used catalysts was evaluated by TGA on a Mettler Toledo TGA/DSC1 thermobalance under airflow (100 mL min^{-1}) with a heating rate of 5 °C min^{-1} up to 1000 °C. The value of coke deposition is given as

$$C_{\text{dep}}\ (\text{wt\%}) = \frac{m_{\text{coke}}}{m_{\text{used catalyst}}} \times 100$$

m_{coke} is the mass of coke deposited on the catalyst, calculated from the weight loss measured by TGA in the range of temperatures corresponding to carbonaceous matter combustion (see Section 3.3), and $m_{\text{used catalyst}}$ is the mass of catalyst calculated from the weight remaining after the TG analysis, considering the dilution of the catalyst into SiC.

Used catalysts were also characterized by XRD using the abovementioned methods to determine metal sintering and coke nature. In order to analyse the morphology of carbon deposits formed on used catalysts, scanning electron microscopy (SEM) was performed on a Phillips XL30 Environmental Scanning Electron Microscope equipped with a tungsten filament and an accelerating voltage of 15 kV. Moreover, the structure of carbon deposits was studied by Raman spectroscopy on a HORIBA Jobin Yvon LabRAM HR spectrometer equipped with an OLYMPUS BX41 microscope (50× magnification) and a thermoelectrically cooled CCD detector (−80 °C). The samples were excited with the 632.8 nm He–Ne line and the spectra acquisition consisted of five accumulations of 30 s.

3. Results and discussion

3.1. Characterization of the Mg- and Ca-modified Cu–Ni/SiO_2 catalysts

Table 1 summarizes the physicochemical properties of the prepared supports and the corresponding catalysts used in this work. Regarding calcined supports, the incorporation of Ca or Mg considerably reduces silica textural properties as the loading is increased. This effect is more pronounced in the case of Ca addition, as observed elsewhere for SBA-15 based supports [18], which may be related to more support surface covering due to lower density of CaO in comparison to MgO. As expected, the incorporation

Table 1
Physicochemical properties of Mg- and Ca-modified calcined supports and reduced catalysts.

Sample	Cu[a] (wt%)	Ni[a] (wt%)	Mg or Ca[a] (wt%)	S_{BET} ($m^2\ g^{-1}$)	V_{pore}[b] ($cm^3\ g^{-1}$)	D_{pore}[c] (nm)	D_{Ni}[d] (nm)
SiO_2	–	–	0.0	273	1.58	32.5	–
Mg10-S	–	–	10.4	186	1.38	30.2	–
Mg20-S	–	–	18.2	156	0.94	26.1	–
Ca10-S	–	–	9.3	160	0.96	27.0	–
Ca20-S	–	–	20.2	127	0.70	24.3	–
CuNi/S	2.0	6.5	0.0	228	1.27	26.3	20.1
CuNi/Mg10-S	2.0	7.5	9.4	140	0.69	23.7	4.6
CuNi/Mg20-S	2.0	6.5	16.6	120	0.47	17.5	6.0
CuNi/Ca10-S	1.8	6.6	8.5	123	0.56	23.9	6.2
CuNi/Ca20-S	1.8	6.8	18.5	116	0.45	15.5	8.2

[a] ICP-AES measurements.
[b] Determined at P/Po = 0.98.
[c] Calculated through the maximum of the BJH pore size distribution.
[d] Calculated from XRD measurements.

of the Cu–Ni phase also diminishes the textural properties of the corresponding supports.

Fig. 1 shows XRD patterns of the reduced Cu–Ni catalysts supported on Ca- or Mg-modified silica. Diffractograms show only peaks corresponding to cubic Ni (JCPDS 04-0850), at $2\theta = 44.5$, 51.8 and 76.3°. Reflections corresponding to Cu cannot be distinguished because of the low loading in the samples, which leads to a dilution effect of Cu into Ni phase, as previously discussed [8]. MgO and CaO are highly dispersed after the Cu–Ni phase incorporation, as neither MgO nor CaO peaks are observed in the catalysts diffractograms. In comparison to the pattern corresponding to CuNi/S catalyst, peaks become significantly smaller and wider for samples containing Mg or Ca. This indicates the presence of smaller Ni crystallites over Mg- and Ca-modified silica and therefore the dispersion of Cu–Ni phase on the silica surface has been improved. Regarding mean crystallites size calculated by Debye–Scherrer equation, CuNi/S unpromoted catalyst has relatively large Ni crystallites (20.1 nm), while they are significantly smaller in modified samples (Table 1). This effect is slightly more pronounced in the case of Mg-modified catalysts in comparison to Ca-promoted ones, which may be due to higher surface area available in the support (see Table 1) to accommodate the Cu–Ni phase. On the other hand, an increase of alkaline-earth content leads to slightly larger Ni crystallites, which

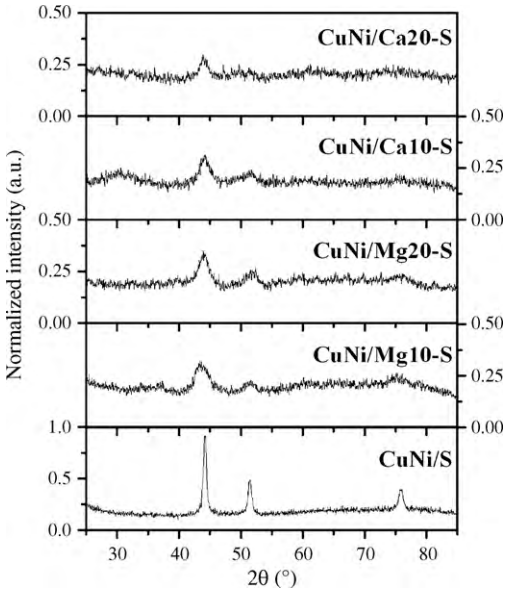

Fig. 1. XRD diffractograms of reduced Mg- and Ca-modified $CuNi/SiO_2$ catalysts. For comparative purposes, diffractograms have been normalized to the maximum intensity of CuNi/S profile.

may be also explained by a decrease of the support surface area as alkaline-earth loading increases.

The above-mentioned differences in metallic crystals size could be verified by TEM. Fig. 2 shows the micrographs corresponding to the reduced catalysts. On CuNi/S sample (Fig. 2a), metallic particles (dark zones) within a wide range of sizes, between 5 and 70 nm, can be found. However, promoted catalysts (Fig. 2b–e) show metallic particles significantly smaller, ranging from 2 to 10 nm, which agrees with the dispersing effect of Mg and Ca observed by XRD. EDXS analysis (not shown here) proved the presence of both Cu and Ni within each metallic particle, as previously reported [8,18,19], which explains the different values of metal particles size observed by TEM in comparison to those calculated from XRD.

Fig. 3 shows the hydrogen TPR profiles of the Cu–Ni catalysts. Fig. 3a shows the hydrogen TPR profiles of the Cu–Ni catalysts. Sample supported on bare silica, CuNi/S, shows a peak with maximum at 209 °C and a shoulder at lower temperatures. While Cu/SiO_2 catalysts are characterized by one peak around 190–230 °C, corresponding to the reduction of bulk CuO particles to Cu^0, and Ni/SiO_2 catalysts present one characteristic reduction peak around 310–410 °C, due to the reduction of bulk NiO particles to Ni^0, $Cu–Ni/SiO_2$ catalysts typically show one reduction zone between 200 and 260 °C. This has been ascribed to superposition of a low temperature peak corresponding to CuO particles reduction and a higher temperature peak attributed to NiO particles reduction, as the presence of Cu significantly decreases NiO reduction temperature [7,20–23]. So, the CuNi/S sample profile corresponds to the reduction of CuO and NiO particles with weak metal–support interaction. For this kind of catalysts, however, higher interaction between Cu^{2+} or Ni^{2+} and SiO_2, associated to reduction peaks at higher temperature, has also been reported in literature [20,24–26]. On the other side, Mg and Ca-promoted $Ni–Cu/SiO_2$ catalysts present two reduction zones. The first one, below 350 °C, corresponds to the reduction of CuO–NiO particles with low metal–support interaction (similar to that found on CuNi/S sample), and the second one, from 350 to 700 °C, may be related with the reduction of CuO–NiO phase strongly interacting with the support. Table 2 shows the contribution of each reduction

Table 2
Area contribution of reduction zones below and over 350 °C to the catalysts H_2-TPR profiles.

Sample	Low temperature zone area (%)	High temperature zone area (%)
CuNi/S	100.0	0.0
CuNi/Mg10-S	14.9	85.1
CuNi/Mg20-S	16.7	83.3
CuNi/Ca10-S	20.0	80.0
CuNi/Ca20-S	21.9	78.1

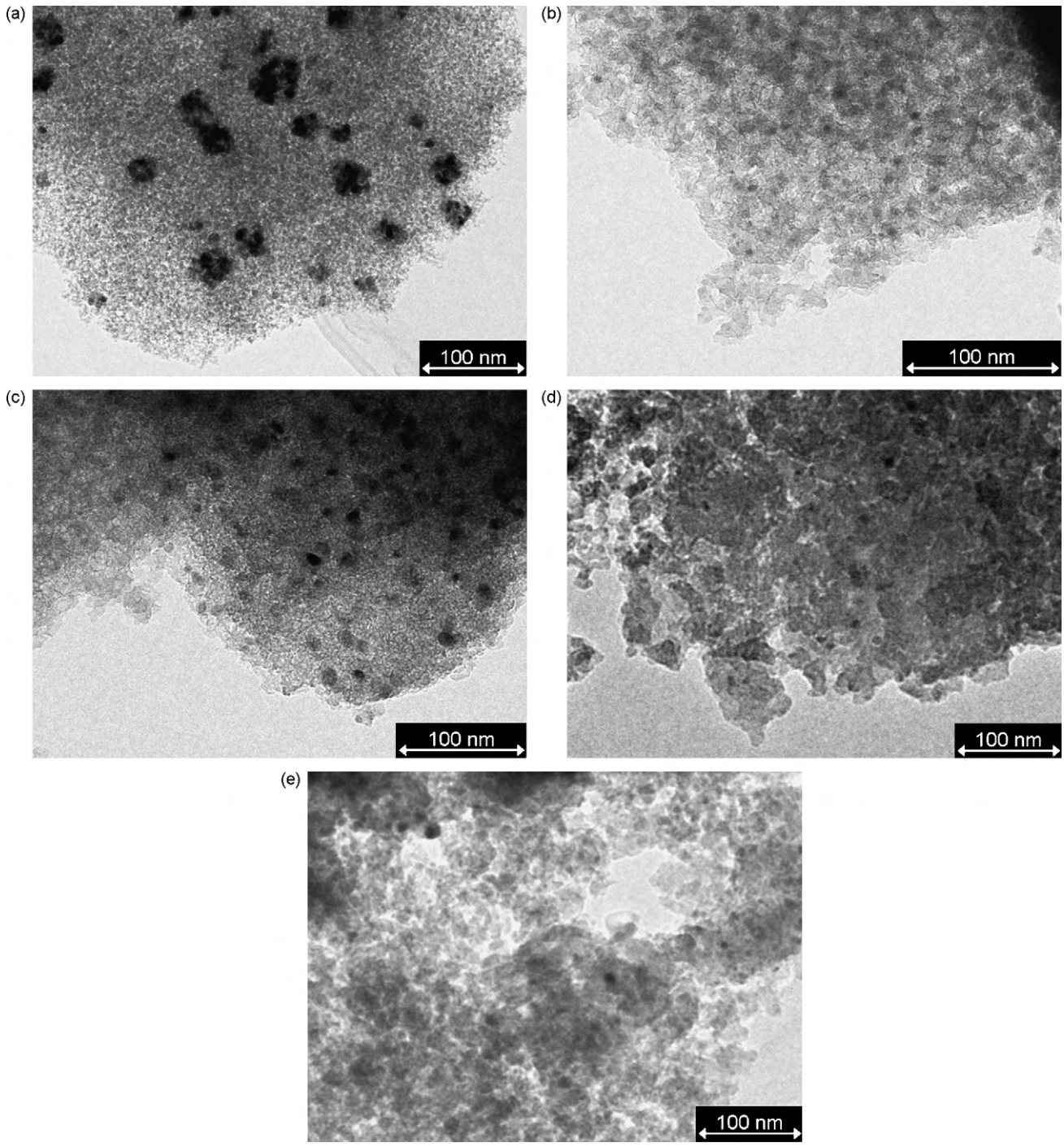

Fig. 2. TEM images of Mg and Ca-modified CuNi/SiO_2 catalysts: (a) CuNi/S, (b) CuNi/Mg10-S, (c) CuNi/Mg20-S, (d) CuNi/Ca10-S and (e) CuNi/Ca20-S.

zone to the profiles total area. It can be observed how the area under the low temperature reduction zone decreases while the area under the high temperature reduction zone increases upon the incorporation of Mg and Ca, which accounts for the smaller Ni crystallites formed in the modified catalysts, as observed by XRD. According to maximum reduction temperatures, strengthening of the metal–support interaction by calcium is slightly higher than in the case of magnesium, which may be due to the stronger basicity of CaO [27]. However, Mg-promoted samples show lower proportion of Cu–Ni phase weakly interacting with the support (reduction temperature bellow 350 °C), which coincides with the smaller mean Ni crystallites size in Table 1. On the other hand, when the alkaline-earth content is increased from 10 to 20 wt%, metal–support interaction becomes weaker, probably as a consequence of an excessive amount covering the silica surface. A similar trend has been observed for Ni catalysts supported on alumina [17,28].

3.2. Catalytic results on ethanol steam reforming

Catalytic activity and selectivity in the ethanol steam reforming, as well as carbon percentage deposited after 3 h of time on stream, are shown in Table 3. All the catalysts reach almost complete ethanol conversion. Compared to the CuNi/S sample, both

Table 3
Catalytic results on ethanol steam reforming over Mg- and Ca-modified CuNi/SiO_2 catalysts (T = 600 °C, atmospheric pressure, $R_{H_2O/EtOH}$ = 3.7 mol/mol, WHSV = 12.7 h^{-1}, time on stream = 3 h).

Catalyst	Conversion (mol%)		Selectivity (mol%)				C_{dep} (wt%)
	EtOH	H_2O	H_2	CO_2	CO	CH_4	
CuNi/S	99.9	36.3	69.9	49.9	17.4	32.7	58.4
CuNi/Mg10-S	100.0	46.7	84.8	55.7	28.1	16.2	34.4
CuNi/Mg20-S	99.9	41.6	80.8	48.9	29.6	21.5	36.1
CuNi/Ca10-S	99.9	43.5	78.1	52.6	25.3	22.1	26.3
CuNi/Ca20-S	99.9	37.6	74.9	47.3	27.1	25.6	32.3

Mg- and Ca-modified Cu–Ni catalysts achieve higher water conversion, although this is more pronounced in the case of Mg addition. Regarding products distribution, lower methane selectivity is found for Mg- and Ca-modified catalysts. This is indicative of higher activity in the methane steam reforming step within the reaction pathway [7], since according to the literature [10], the hydrocarbon or ethanol activation occurs more readily on small metallic particles, present onto Ca- and Mg-modified silica, than on big ones found in CuNi/S catalyst. Therefore, higher hydrogen selectivity is reached on promoted samples, but carbon monoxide selectivity also increases, which indicates that these catalysts are also active in the reverse water-gas shift reaction, expected to occur at the present conditions [29].

Highest hydrogen selectivities (80.8–84.8 mol%) are reached with Cu–Ni/Mg–SiO_2 catalysts, which is in accordance with the lower methane selectivity and high water conversion. This completely agrees with the smaller Ni crystallites found in these catalysts, as calculated from XRD (Table 1), and shows that incorporation of Mg to SiO_2 support leads to better dispersing effect of the Cu–Ni active phase than incorporation of Ca. Moreover, as alkaline-earth loading increases from 10 to 20 wt%, hydrogen selectivity decreases as a consequence of lower metallic dispersion.

On the other hand, Table 3 shows relatively high coke deposition (58.4 wt%) on CuNi/S sample, while carbon formation was significantly reduced in catalysts containing Mg and Ca. This may be attributed to both an increase in the basicity of the support, which unfavours the formation of ethylene as intermediate product (a hard precursor of coke), and an improvement of the Ni dispersion (smaller Cu–Ni metallic particles), which negatively affects to the formation mechanism of carbon nanofibres, typically found on this kind of catalysts [10,30–33]. The strengthening of the interaction between the Cu–Ni phase and the support must be also taken into account, since this would prevent the formation of large ensembles of Ni by sintering during reaction [30]. In this case, the lowest carbon deposition was achieved with Ca-promoted samples, concretely with the CuNi/Ca10-S catalyst (26.3 wt%), probably due to the stronger basicity of CaO in comparison to MgO [33]. On the other hand, an increase in alkaline-earth content from 10 to 20 wt% leads to higher coke deposition, which may be related to an increase of the metal particle size.

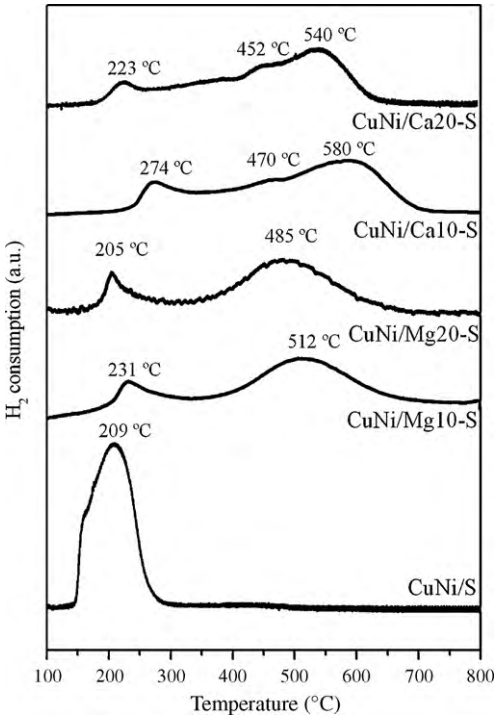

Fig. 3. TPR profiles of calcined Mg- and Ca-modified CuNi/SiO_2 catalysts.

3.3. Characterization of coke deposits on Mg- and Ca-modified Cu–Ni/SiO_2 catalysts

Fig. 4 shows SEM images of the used catalysts revealing that the solid carbon product consists of nanofibres on the particles of catalyst. Images showing particles with high amount of coke were selected for the sake of clarity. The fact that no deactivation was observed during reaction agrees with the nanofibres being the prevailing kind of coke. So, the morphology of the deposits found on the different catalysts is similar. Comparing catalysts, it seems that the carbon fibres on CuNi/S sample are wider than those observed on the CuNi/Mg20-S and CuNi/Ca20-S catalysts, which can be explained by the finding that the width of the nanofibres is related to the metal particle size [34]. However, taking into account the heterogeneity in size and shape of the nanofibres found on each catalyst, it is difficult to point out more significant differences between the deposits formed on the different samples from microscopy.

TG analyses of the used catalysts showed some differences concerning stability of the carbon deposits formed during ethanol steam reforming. Fig. 5 shows derivative thermograms, pointing out the temperatures at which maximum carbonaceous matter combustion rate takes place under oxidative conditions for each used catalyst. All the samples show a wide DTG profile with peaks maxima between 536 and 551 °C, except for the used CuNi/S catalyst, which presents also another peak around 588 °C in a wide DTG profile, suggesting the presence of more stable carbon deposits. Regarding promoted samples, although differences are not so significant, the order of temperatures at which coke combustion occurs is: CuNi/Ca10-S < CuNi/Ca20-S < CuNi/Mg10-S < CuNi/Mg20-S. This fact may suggest a role of MgO and mainly of CaO in catalyzing the combustion of the deposited carbon, according to literature [33], although it may also be due to differences in the nature of carbonaceous deposits. It is well known that amorphous carbon is more reactive, while graphitic carbon needs higher temperature to be removed. According to Galetti et al. [35], peaks at low temperature are ascribed to carbon on nickel surface, whereas the peaks above 550 °C are ascribed to coke deposits in the fila-

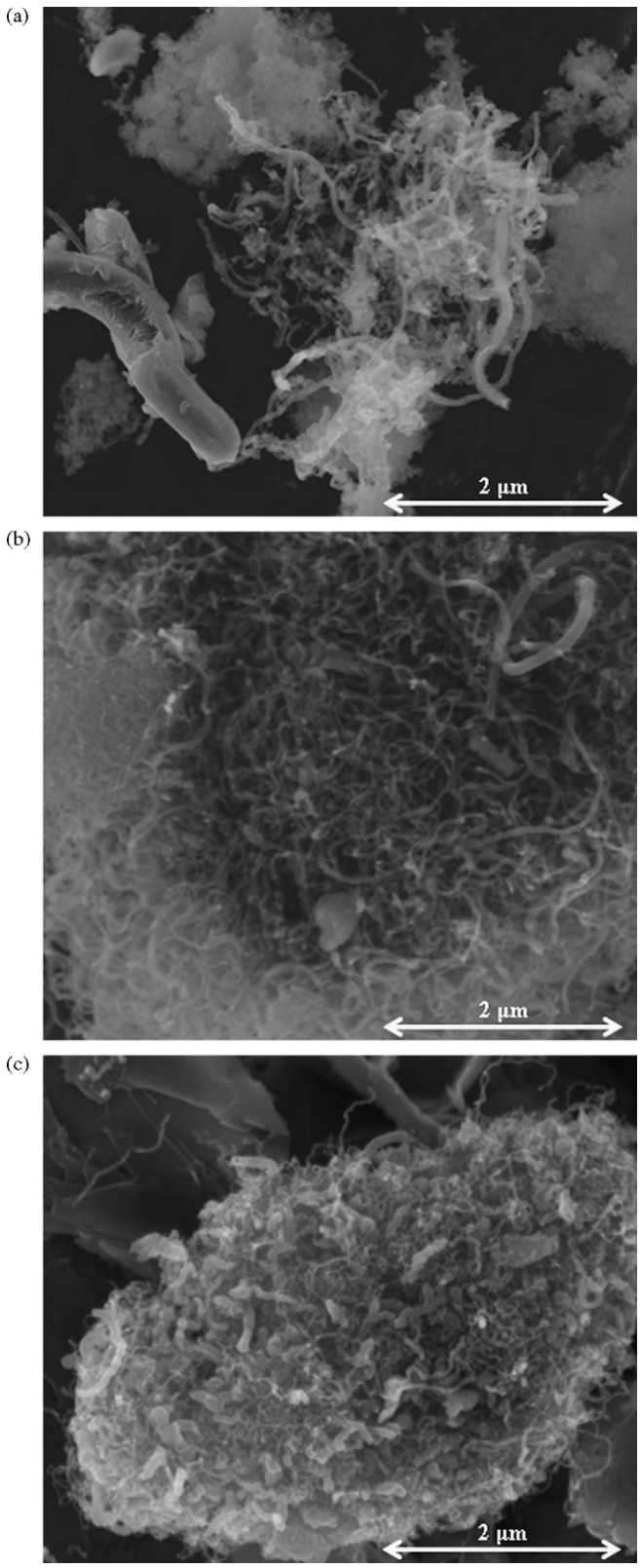

Fig. 4. SEM images of used Mg and Ca-modified CuNi/SiO_2 catalysts: (a) CuNi/S, (b) CuNi/Mg20-S and (c) CuNi/Ca20-S.

ment form with different degree of graphitization. Any possible carbonate formation could not be detected by TGA. Decomposition of $CaCO_3$ and $MgCO_3$ occurs around 655 and 430 °C, respectively [36]. At those temperatures, a peak should arise in the DTA profiles if carbonates were present on the catalysts, but no peak or shoulder can be observed. This indicates that, in case of CO_2 adsorption on the catalyst as carbonates, the amount is small enough to not interfere with the TGA signal.

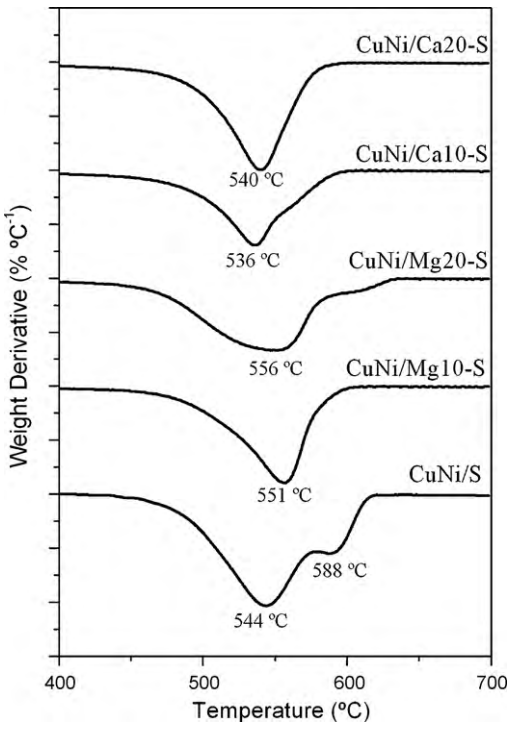

Fig. 5. Derivative TGA of used Mg- and Ca-promoted CuNi/SiO_2 catalysts performed under airflow.

Fig. 6 compares the XRD patterns of used catalysts. A break has been introduced between $2\theta = 30$ and 40° in order to simplify diffractograms, as only peaks corresponding to silicon carbide (used to dilute catalysts during reaction) appeared in this range. Due to dilution effect, XRD signal corresponding to the Ni phase in these samples is much less intense in comparison to that of

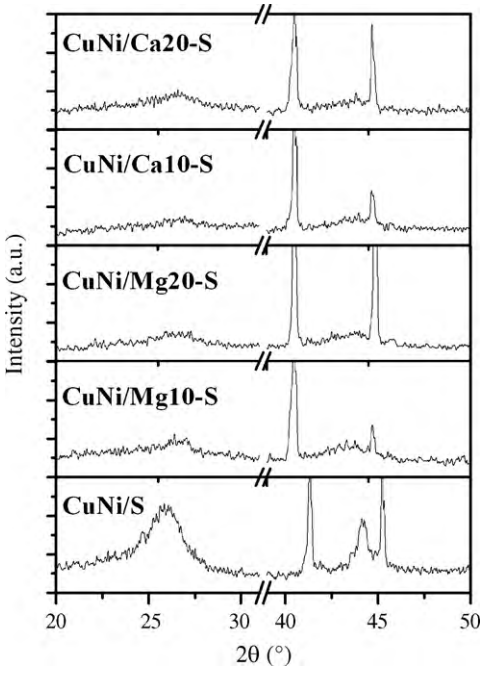

Fig. 6. XRD diffractograms of used Mg- and Ca-promoted CuNi/SiO_2 catalysts.

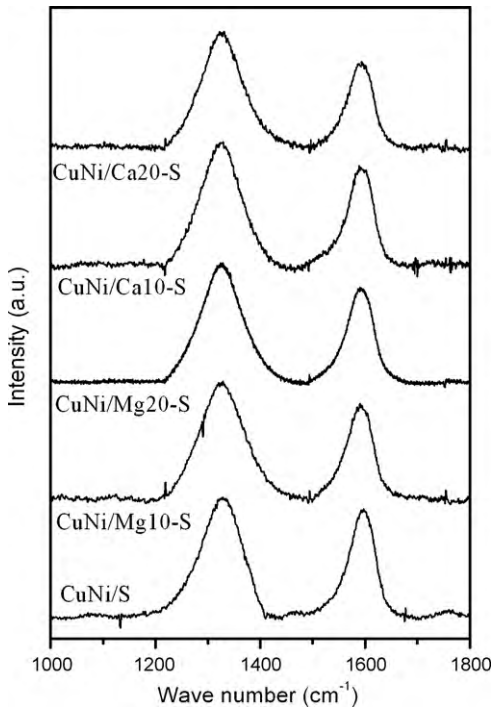

Fig. 7. Raman spectra of used Mg- and Ca-promoted CuNi/SiO_2 catalysts.

reduced samples (Fig. 1), resulting in noisy diffractograms. Intense peaks corresponding to this SiC can still be observed at $2\theta = 41.3$ and 45.2° (JCPDS 75-0254). Reflections corresponding to Cu or Ni species cannot be properly distinguished, except for the CuNi/S sample, where the main peak of metallic Ni at $2\theta = 44.3°$ is observed with Ni crystallites size of 24.1 nm (calculated from Scherrer equation). Compared to the Ni particle size found for the fresh sample (20.1 nm, see Table 1), this evidences sintering of the metallic phase during reaction, in accordance with the low metal–support interaction observed by TPR. On the other hand, the reflection (0 0 2) of graphitic carbon at $2\theta = 26.5°$ (JCPDS: 41-1487) is also detected in all the samples. This peak is very intense for CuNi/S sample indicating high formation of graphitic carbon in agreement with the TGA results (Fig. 5).

Raman spectroscopy has shown to be a powerful technique for characterizing the structure of carbonaceous materials [9,35,37–40]. Thus, the Raman spectra in the range 1000–1800 cm^{-1} of the used samples are presented in Fig. 7. Two bands centred at ca. 1330 and 1590 cm^{-1} are visible, which are known as D-band and G-band, respectively. G-band is attributed to the stretching mode of carbon sp^2 bonds of ordered graphite, while the D-band is ascribed to the vibrations of carbon atoms with dangling bonds in disordered carbonaceous species [35]. D-band is more intense than G-band, indicating a predominance of disordered carbon, such as amorphous or defective filamentous. Carbon structures seem to be similar on all the catalysts, but some differences in the relative intensity of the bands can be observed. A quantitative characterization of the disordering degree of the carbonaceous materials can be made based on the integrated intensity of the D- and G-bands though the calculation of the microcrystalline planar size (L_a), i.e. the mean crystal domain size along the basal planes of deposited carbon, by applying Tuinstra and Koenig's law: L_a (nm) = 4.4 I_G/I_D [41]. Larger L_a value implies higher ordering degree of the carbonaceous materials. As it can be observed in Table 4, L_a is estimated to be 2.6 nm for CuNi/S sample, which is similar to that previously reported for some Cu–Ni/SiO_2 catalysts [38]. However, the presence of alkaline-earth elements in the catalyst promotes the formation of disordered carbon, attending to lower L_a values, mainly in the case of Ca in comparison to Mg, so that it may be probably related to the higher basicity of Ca [33]. Thus, these results are in complete agreement with those obtained by TGA (Fig. 5), since the presence of a less ordered coke on promoted catalysts, leaded to a lower carbon oxidation temperature.

Table 4
Raman spectroscopic parameters of carbonaceous species deposited on used Mg- and Ca-promoted CuNi/SiO_2 catalysts.

Sample	D-band position (cm^{-1})	G-band position (cm^{-1})	L_a (nm)
CuNi/S	1329	1596	2.62
CuNi/Mg10-S	1326	1590	2.27
CuNi/Mg20-S	1326	1592	2.31
CuNi/Ca10-S	1326	1588	2.10
CuNi/Ca20-S	1326	1592	2.10

Raman spectroscopy analyses of the samples recovered after the TG analysis were also carried out, but no signal corresponding to carbonaceous species was detected for any of the samples. If remaining carbon was still present on the samples, the amount cannot be detectable by Raman spectroscopy.

Summing up, according to SEM and XRD (Figs. 4 and 6), coke formed on the different samples studied in this work shows filamentous morphology and graphitic nature in all the cases, but with different degree of ordering. Raman spectroscopy (Fig. 7) demonstrates the presence of less ordered coke on Mg- and Ca-promoted catalysts, which is known to be more reactive, in complete agreement with the results obtained by TGA (Fig. 5). A reactive carbon is easier to remove (for example, by gasification) during ethanol steam reforming, so that coke deposition is can be decreased with Ca and Mg-promoted catalysts. In fact, the order of temperatures for carbon removal obtained by TGA coincides with the order of amount of carbon deposited: CuNi/Ca10-S < CuNi/Ca20-S < CuNi/Mg10-S < CuNi/Mg20-S < CuNi/S.

Formation of less ordered carbon deposits by Mg- or Ca-modification of CuNi/SiO_2 catalyst may be related to electronic perturbations in the dispersed metallic phase by varying the nature of the support, which has been reported to impact on carbon fibres dimensions, morphology or lattice structure [42]. In addition, ordered filamentous carbon mainly forms over faceted metal particles of definite shape, whose size is close to the diameter of carbon filaments growing on them [34,42,43]. The smaller metal particles found in the promoted catalysts in comparison to the CuNi/S sample, together with the higher metal–support interaction which should diminish sintering, implies lower proportion of faceted particles [43]. This fact may hinder ordered graphite sheets growth and results in narrower nanofibres (Fig. 4) with consequent higher availability of edge sites, considered as a breakdown of symmetry [42,44,45].

4. Conclusions

Incorporation of alkaline-earth elements (Mg and Ca) to the silica support of Cu–Ni/SiO_2 catalysts has been performed and resulting catalysts have been evaluated for hydrogen production through ethanol steam reforming. Both Mg and Ca addition improved the dispersion of the Cu–Ni metallic phase and strengthened metal–support interaction, as found from H_2-TPR and XRD analyses. Consequently, the catalytic behaviour was enhanced, so that Mg- and Ca-modified Cu–Ni/SiO_2 catalysts exhibited high reforming activity. Mg-promoted catalysts achieve the highest hydrogen selectivity because of smaller Ni crystallites size, which is one of the main factors affecting catalytic activity.

Moreover, coke resistance ability was also improved, as Ca and Mg promote the formation of less ordered carbon, which is more

reactive and easier to remove by gasification during ethanol steam reforming. In this case, Ca-modified catalysts produce the lowest carbon deposition. This may be related to both an increase of the basicity of the catalysts and a reduction of active phase particle size, since carbon formation occurs mainly when the metal clusters are greater than a critical value. So, one can conclude that these factors are particularly significant in the design of anti-carbon deposition catalysts.

References

[1] K.A. Gray, L. Zhao, M. Emptage, Bioethanol, Curr. Opin. Chem. Biol. 10 (2006) 141–146.
[2] A. Haryanto, S. Fernando, N. Murali, S. Adhikari, Current status of hydrogen production techniques by steam reforming of ethanol: a review, Energy Fuels 19 (2005) 2098–2106.
[3] M. Benito, J.L. Sanz, R. Isabel, R. Padilla, R. Arjona, L. Daza, Bio-ethanol steam reforming: insights on the mechanism for hydrogen production, J. Power Sources 151 (2005) 11–17.
[4] D.L. Trimm, Coke formation and minimisation during steam reforming reactions, Catal. Today 37 (1997) 233–238.
[5] B.C. Zhang, Y. Li, W.J. Cai, X.L. Tang, Y.D. Xu, W.J. Shen, Steam reforming of ethanol over Ni–Cu/CeO_2 catalyst, Chin. J. Catal. 27 (2006) 567–572.
[6] F. Wang, Y. Li, W.J. Cai, E. Zhan, X. Mu, W.J. Shen, Ethanol steam reforming over Ni and Ni–Cu catalysts, Catal. Today 146 (2009) 31–36.
[7] A.J. Vizcaíno, A. Carrero, J.A. Calles, Hydrogen production by ethanol steam reforming over Cu–Ni supported catalysts, Int. J. Hydrogen Energy 32 (2007) 1450–1461.
[8] A. Carrero, J.A. Calles, A.J. Vizcaíno, Hydrogen production by ethanol steam reforming over Cu–Ni/SBA-15 supported catalysts prepared by direct synthesis and impregnation, Appl. Catal. A: Gen. 327 (2007) 82–94.
[9] S.H. Yoon, S. Lim, S.H. Hong, W. Qiao, D. Whitehurst, I. Mochida, B. An, K. Yokogawa, A conceptual model for the structure of catalytically grown carbon nano-fibers, Carbon 43 (2005) 1828–1838.
[10] F. Aupretre, C. Descorme, D. Duprez, D. Casanave, D. Uzio, Ethanol steam reforming over $Mg_xNi_{1-x}Al_2O_3$ spinel oxide-supported Rh catalysts, J. Catal. 233 (2005) 464–477.
[11] F. Pompeo, N.N. Nichio, O.A. Ferretti, D. Resasco, Study of Ni catalysts on different supports to obtain synthesis gas, Int. J. Hydrogen Energy 30 (2005) 1399–1405.
[12] F.J. Mariño, E.G. Cerella, S. Duhalde, M. Jobbagy, M.A. Laborde, Hydrogen from steam reforming of ethanol: characterization and performance of copper–nickel supported catalysts, Int. J. Hydrogen Energy 23 (1998) 1095–1101.
[13] F. Mariño, M. Boveri, G. Baronetti, M. Laborde, Hydrogen production from steam reforming of bioethanol using Cu/Ni/K/γ-Al_2O_3 catalysts: effect of Ni, Int. J. Hydrogen Energy 26 (2001) 665–668.
[14] P. Chen, Z.Y. Hou, X.M. Zheng, Production of synthesis gas via methane reforming with CO_2 on Ni/SiO_2 catalysts promoted by alkali and alkaline earth metals, Chin. J. Chem. 23 (2005) 847–851.
[15] J.S. Lisboa, D.C.R.M. Santos, F.B. Passos, F.B. Noronha, Influence of the addition of promoters to steam reforming catalysts, Catal. Today 101 (2005) 15–21.
[16] Z. Cheng, Q. Wu, J. Li, Q. Zhu, Effects of promoters and preparation procedures on reforming of methane with carbon dioxide over Ni/Al_2O_3 catalyst, Catal. Today 30 (1996) 147–155.
[17] Z. Hou, O. Yokota, T. Tanaka, T. Yashima, Characterization of Ca-promoted Ni/α-Al_2O_3 catalyst for CH_4 reforming with CO_2, Appl. Catal. A: Gen. 253 (2003) 381–387.
[18] A.J. Vizcaíno, A. Carrero, J.A. Calles, Ethanol steam reforming on Mg- and Ca-modified Cu–Ni/SBA-15 catalysts, Catal. Today 146 (2009) 63–70.
[19] J.A. Calles, A. Carrero, A.J. Vizcaíno, Ce and La modification of mesoporous Cu–Ni/SBA-15 catalysts for hydrogen production through ethanol steam reforming, Micropor. Mesopor. Mater. 119 (2009) 200–207.
[20] A. Jones, B.D. McNicol, Temperature-programmed Reduction for Solid Materials Characterization, Marcel-Dekker, New York, 1986.
[21] D.S. Brands, E.K. Poels, A. Bliek, Ester hydrogenolysis over promoted Cu/SiO_2 catalysts, Appl. Catal. A: Gen. 184 (1999) 279–289.
[22] C.I. Meyer, A.J. Marchi, A. Monzón, T.F. Garetto, Deactivation and regeneration of Cu/SiO_2 catalyst in the hydrogenation of maleic anhydride: kinetic modelling, Appl. Catal. A: Gen. 367 (2009) 122–129.
[23] A. Khan, P.G. Smirniotis, Relationship between temperature-programmed reduction profile and activity of modified ferrite-based catalysts for WGS reaction, J. Mol. Catal. A: Chem. 280 (2008) 43–51.
[24] G.P. Babu, R.S. Murthy, Influence of metal–support interactions on Ni–silica catalyst reduction behaviours: TPR studies, in: B. Viswanathan, C.N. Pillai (Eds.), Recent Developments in Catalysis: Theory and Practice, Narosa Publishing House, New Delhi, 1990.
[25] Y.H. Choi, W.Y. Lee, Effect of second metals and Cu content on catalyst performance of Ni–Cu/SiO_2 in the hydrodechlorination of 1,1,2-trichloroethane into vinyl chloride monomer, J. Mol. Catal. A: Chem. 174 (2001) 193–204.
[26] E.D. Guerreiro, O.F. Gorriz, J.B. Rivarola, L.A. Arrúa, Cu/SiO_2 catalysts for methanol to methyl formate dehydrogenation: a comparative study using different preparation techniques, Appl. Catal. A: Gen. 204 (2000) 33–48.
[27] L.B. Råberg, M.B. Jensen, U. Olsbye, C. Daniel, S. Haag, C. Mirodatos, A. OlafsenSjåstad, Propane dry reforming to synthesis gas over Ni-based catalysts: influence of support and operating parameters on catalyst activity and stability, J. Catal. 249 (2007) 250–260.
[28] J.A.C. Dias, J.M. Assaf, Influence of calcium content in Ni/CaO/γ-Al_2O_3 catalysts for CO_2-reforming of methane, Catal. Today 85 (2003) 59–68.
[29] V. Mas, R. Kipreos, N. Amadeo, M. Laborde, Thermodynamic analysis of ethanol/water system with the stoichiometric method, Int. J. Hydrogen Energy 31 (2006) 21–28.
[30] Z. Hou, O. Yokota, T. Tanaka, T. Yashima, A novel KCaNi/α-Al_2O_3 catalyst for CH_4 reforming with CO_2, Catal. Lett. 87 (2003) 37–42.
[31] H.W. Chen, C.Y. Wang, C.H. Yu, L.T. Tseng, P.H. Liao, Carbon dioxide reforming of methane reaction catalyzed by stable nickel copper catalysts, Catal. Today 97 (2004) 173–180.
[32] I. Alstrup, M.T. Tavares, C.A. Bernardo, O. Sørensen, J.R. Rostrup-Nielsen, Carbon formation on nickel and nickel–copper alloy catalysts, Mater. Corros. 49 (1998) 367–372.
[33] N. Alarcón, X. García, M.A. Centeno, P. Ruiz, A. Gordon, New effects during steam gasification of naphthalene: the synergy between CaO and MgO during the catalytic reaction, Appl. Catal. A: Gen. 267 (2004) 251–265.
[34] A.R. Naghash, Z. Xu, T.H. Etsell, Coprecipitation of nickel–copper–aluminum takovite as catalyst precursors for simultaneous production of carbon nanofibers and hydrogen, Chem. Matter 17 (2005) 815–821.
[35] A.E. Galetti, M.F. Gómez, L.A. Arrúa, M.C. Abello, Hydrogen production by ethanol reforming over NiZnAl catalysts: influence of Ce addition on carbon deposition, Appl. Catal. A: Gen. 348 (2008) 94–102.
[36] B.V. L'vov, Mechanism and kinetics of thermal decomposition of carbonates, Thermochim. Acta 386 (2002) 1–16.
[37] J. Llorca, N. Homs, J. Sales, P. Ramírez de la, Piscina, Efficient production of hydrogen over supported cobalt catalysts from ethanol steam reforming, J. Catal. 209 (2002) 306–317.
[38] M.J. Lázaro, Y. Echegoyen, I. Suelves, J.M. Palacios, R. Moliner, Decomposition of methane over Ni–SiO_2 and Ni–Cu–SiO_2 catalysts: effect of catalyst preparation method, Appl. Catal. A: Gen. 329 (2007) 22–29.
[39] H. Song, U.S. Ozkan, Ethanol steam reforming over Co-based catalysts: role of oxygen mobility, J. Catal. 261 (2009) 66–74.
[40] J. Bian, M. Xiao, S.J. Wang, Y.X. Lu, Y.Z. Meng, Graphite oxide as a novel host material of catalytically active Cu–Ni bimetallic nanoparticles, Catal. Commun. 10 (2009) 1529–1533.
[41] F. Tuinstra, J.L. Koenig, Raman spectrum of graphite, J. Chem. Phys. 53 (1970) 1126–1130.
[42] C. Park, M.A. Keane, Catalyst support effects in the growth of structured carbon from the decomposition of ethylene over nickel, J. Catal. 221 (2004) 386–399.
[43] G.G. Kuvshinov, Yu.I. Mogilnykh, D.G. Kuvshinov, V.I. Zaikovskii, L.B. Avdeeva, Peculiarities of filamentous carbon formation in methane decomposition on Ni-containing catalysts, Carbon 36 (1998) 87–97.
[44] H.S. Bengaard, J.K. Nørskov, J. Sehested, B.S. Clausen, L.P. Nielsen, A.M. Molenbroek, J.R. Rostrup-Nielsen, Steam reforming and graphite formation on Ni catalysts, J. Catal. 209 (2002) 365–384.
[45] J. Chen, X. Yang, Y. Li, Investigation on the structure and the oxidation activity of the solid carbon produced from catalytic decomposition of methane, Fuel 89 (2010) 943–948.